Basic Experiment on the Integration of Grid-Connected Photovoltaic and Dynamic Wireless Power Transfer

Shogo URANO
Faculty of Science and Technology
Tokyo University of Science
Noda,Japan

Masamichi SUGIZAKI
Faculty of Science and Technology
Tokyo University of Science
Noda,Japan

Takehiro IMURA
Faculty of Science and Technology
Tokyo University of Science
Noda,Japan

Yoichi HORI
Faculty of Science and Technology
Tokyo University of Science
Noda,Japan

***Abstract*— Dynamic Wireless Power Transfer (DWPT) technology is attracting attention as a charging method for Battery Electric Vehicles (BEVs). Among others, the combination of DWPT and renewable energy is believed to indirectly reduce CO_2 emissions from running BEVs. There have been several studies combining PV and DWPT, but they have been limited to simulations and have not yet included experiments. In this paper, we propose for the first time to connect a number of MPPT-controlled PV panels to a grid-connected DC bus and combine them with DWPT. Simulations and experiments using MATLAB/Simulink show that the proposed system can execute DWPT with stable power and overall power conversion efficiency, demonstrating the feasibility and effectiveness of the proposed system.**

Keywords— Dynamic Wireless power transfer, Maximum Power Point Tracking, Photovoltaic, Double-LCC topology

I. INTRODUCTION

As the electrification of automobiles has progressed in recent years and research and development of Battery Electric Vehicles (BEVs) has become more active, the short cruising distance and the high price of the vehicle itself associated with the battery price are some of the issues that need to be addressed for BEVs to become widely used. As a solution to these issues, Static Wireless Power Transfer (SWPT) and Dynamic Wireless Power Transfer (DWPT) have attracted attention as a method of charging BEVs [1] - [7]. Using DWPT to power a BEV while it is running allows for longer distance without quick recharging, etc., and lower cost due to the reduced amount of onboard batteries. In addition, combining DWPT technology with Photovoltaic (PV) power generation can indirectly reduce CO_2 emissions in a running EV. In this case, using power generated by PV installed near the charging lanes that actually consume power would reduce transmission losses and help DWPT absorb PV output fluctuations. Although there have been several studies combining PV and DWPT [8] - [12], few integrated studies of PV and DWPT that have been examined to the experimental stage exist. When considering PV+DWPT, there are on-grid and off-grid systems that are connected to the grid. We will examine grid-connected DWPT for stable DWPT even when PV power generation is unstable. The usefulness and feasibility of the proposed system will be verified based on simulations using MATLAB/Simulink and experiments. In the following chapters, Chapter II describes the outline of the proposed PV+DWPT (grid-connected) system. Chapter III describes the output characteristics and Maximum Power Point Tracking (MPPT) control of the PV system, and Chapter IV describes the DWPT system. Then, Chapter V presents the details of the simulation and experiment of the proposed system, and Chapter VI presents the results of the simulation and experiment. The power conversion efficiency of the entire experimental system is calculated and the effectiveness of the proposed system is shown. And finally, Chapter VII presents the conclusion.

II. PHOTOVOLTAIC + DYNAMIC WIRELESS POWER TRANSFER

A schematic diagram of the PV+DWPT system studied in this paper is shown in Fig. 1. A large number of PV panels installed near the charging lane, such as on the side of the road, are controlled by MPPT through DC/DC converters and directly connected to the DC bus. PV surplus power flows to other inverters and grids through the DC bus. However, in this paper, the AC grid and AC/DC converter are treated as a simplified DC grid, and the impact of reverse power flow on the proposed system is not considered. The inverter is square wave driven at 85 kHz, and the WPT compensation topology is based on the Double-LCC topology, which applies LCL filters with gyrator characteristics on both the transmission and receiving sides.

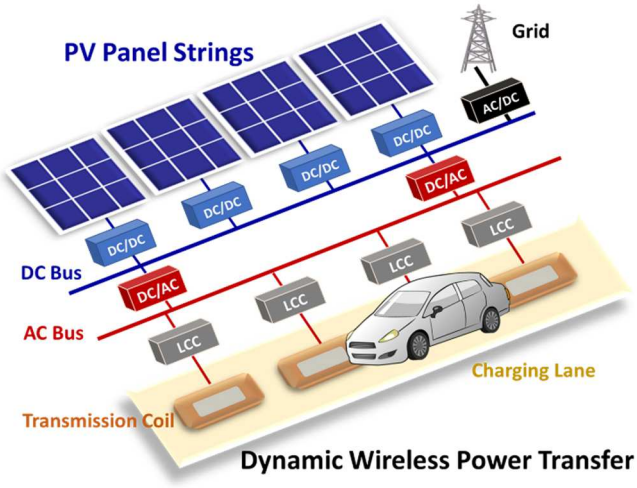

Fig. 1. Schematic diagram of PV+DWPT (grid-connected)

III. PV Panel Output Characteristics and MPPT Control

The PV output power has a Maximum Power Point (MPP) as shown in the P-V curve in Fig. 2. Therefore, the output voltage of the PV (V_{PV}) is controlled so that the output power of the PV (P_{PV}) follows the maximum power point of the PV (P_{MPP}) by changing the duty ratio of the DC/DC boost converter in the subsequent stage using MPPT (Maximum Power Point tracking) control. The MPPT control was performed using the mountain-climbing method of the P&O method, as shown in the flowchart in Fig. 3. First, P_{PV} is calculated from V_{PV} and the output current of the PV (I_{PV}) at each sample time, and the P_{PV} and duty ratio calculated within the sample time of one previous cycle are compared with the current cycle to determine the direction of increase or decrease of duty ratio to be performed in the next sample time. In this way, MPPT control is a method of searching for MPP by changing the duty ratio of the DC/DC converter in the subsequent stage by minute amounts, and by repeating this cycle, P_{MPP} can be followed even if the solar irradiance or the PV panel temperature changes.

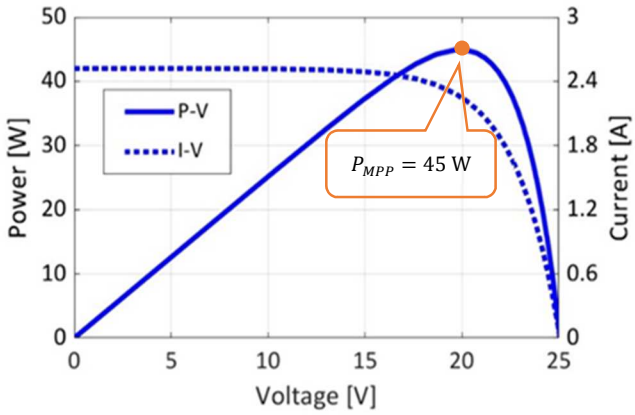

Fig. 2. PV panel output characteristics (P-V, I-V curves)

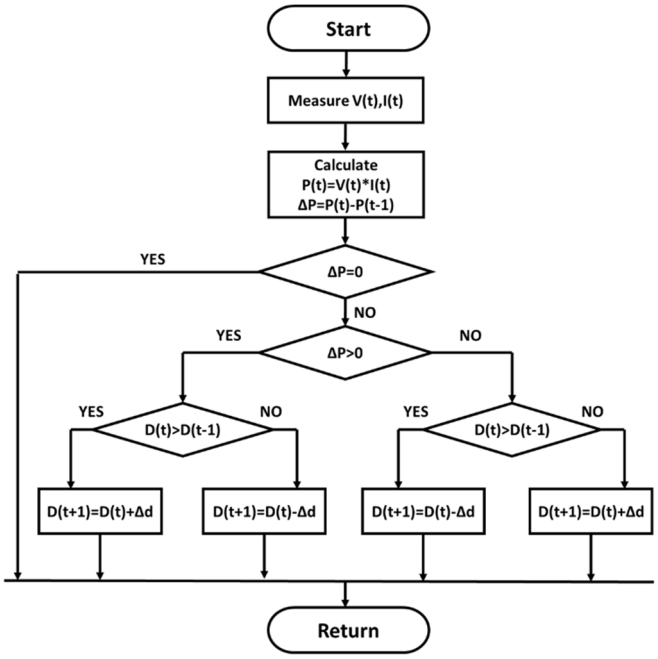

Fig. 3. Flowchart of MPPT control (P&O method)

IV. Dynamic Wireless Power Transfer (DWPT)

A. Double-LCC Topology

Among the various compensation topologies in magnetic field resonant coupling schemes, the Double-LCC topology used for the DWPT in this paper is shown in Fig. 4. The resonance conditions for this scheme are shown in (1) and (2) when the resonance frequency is set to f_0.It can also be seen that in the Double-LCC topology, when $k = 0$, no current flows from the power supply and a circulating current flows in the transmission coil in the opposite direction to that when $k \neq 0$. Therefore, in the Double-LCC topology, even if the voltage continues to be applied when $k = 0$, no large current flows in the transmission coils.

$$\text{(Transmission Side)}: f_0 = \frac{1}{2\pi\sqrt{L_0 C_{1p}}} = \frac{1}{2\pi}\sqrt{\frac{C_{1p}+C_{1s}}{L_1 C_{1p} C_{1s}}} \quad (1)$$

$$\text{(Receiving Side)}: f_0 = \frac{1}{2\pi\sqrt{L'_0 C_{2p}}} = \frac{1}{2\pi}\sqrt{\frac{C_{2p}+C_{2s}}{L_2 C_{2p} C_{2s}}} \quad (2)$$

B. DWPT and Double-LCC Topology

The DWPT system section studied in this paper is shown in Fig. 5. When the Double-LCC topology is used in a DWPT system, multiple transmission coils can be operated simultaneously for a single inverter, even when $k = 0$, because no high current flows in the circuit. However, as the distance of the AC bus between each transmission coil and the inverter increases, the loss due to internal resistance increases and the efficiency at DWPT decreases. In this paper, experiments were conducted with the number of transmission coils per inverter set to three.

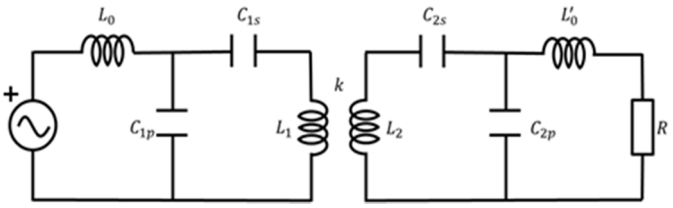

Fig. 4. Basic circuit of Double-LCC topology

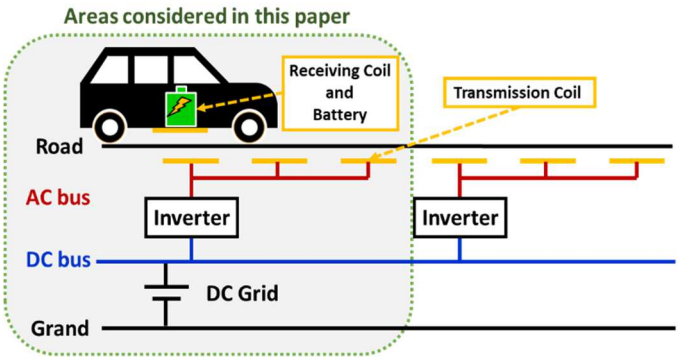

Fig. 5. The DWPT system considered in this paper

V. Circuit Configuration Of the PV+DWPT System

The circuit configuration of the PV+DWPT system studied in this paper is shown in Fig. 6, and the formulas for calculating each parameter of the set amount of electricity are shown in (3)-(7). And the parameters are shown in TABLE I.

$$P_{PV} = V_{PV} \cdot I_{PV} \quad (3)$$
$$P'_{PV} = V_{dc} \cdot I'_{PV} \quad (4)$$
$$P_{dc} = V_{dc} \cdot I_{dc} \quad (5)$$
$$P_{in} = V_{dc} \cdot I_{in} \quad (6)$$
$$P_{out} = V_{out} \cdot I_{out} \quad (7)$$

P_{PV} refers to the output power of the PV and P'_{PV} refers to the power after power conversion by the DC/DC converter. P_{dc} refers to the input power to the DC bus. P_{in} refers to the input power of DWPT, and P_{out} refers to the output power of DWPT. The experimental setup for the PV+DWPT system shown in Fig. 7 and 8 was used. In addition, the simulations and experiments used the parameters listed in Table I. This paper presents two main points. The first point is that the MPPT-controlled PV system is working, and the second point is that the DC bus is controlled at a constant voltage, even if the PV power generation changes, so that when the receiving coil Rx passes through the

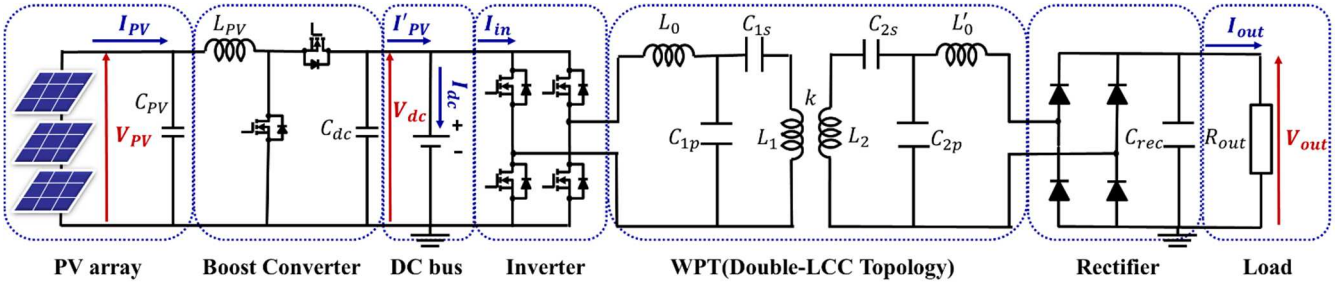

Fig. 6. PV+DWPT system circuit configuration

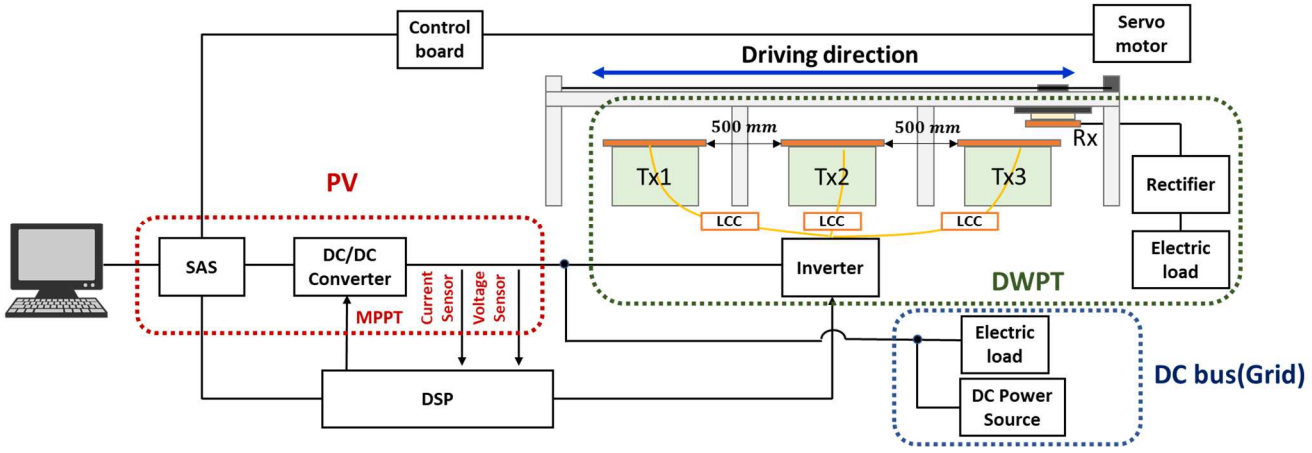

Fig. 7. Overall view of the PV+DWPT experimental system

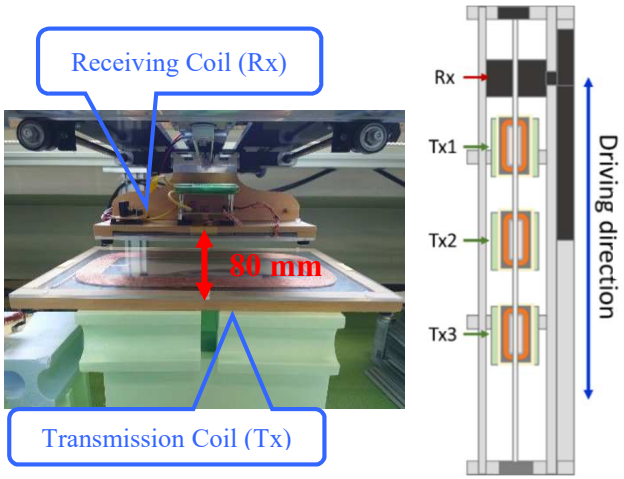

Fig. 8. Appearance of the experimental system (DWPT simulator)

TABLE I. Simulation and Experimental Parameters

(a) PV parameters

f_{dc} [kHz]	Δd	duty sample [s]	f_{dc} [mH]	C_{PV} [μF]	C_{dc} [μF]
10	0.05	0.1	3.5	200	200

(b) DWPT parameters

V_{dc} [V]	f_0 [kHz]	C_{rec} [μF]	R_{out} [Ω]
30	85	500	100

(c) WPT parameters

parameters	Tx1	Tx2	Tx3	Rx
L_0, L'_0 [μH]	53.6	49.8	49.6	49.2
L_1, L_2 [μH]	206.9	206.7	206.4	111.4
C_{1p}, C_{2p} [nF]	65.4	70.4	70.8	71.2
C_{1s}, C_{2s} [nF]	22.9	22.3	22.3	56.4

transmission coils Tx1 ~ Tx3, DWPT can be performed with a stable amount of power. The sizes of the transmission coils Tx1 through Tx3 are all 500 mm × 250 mm, and the size of the receiving coil Rx is 250 mm × 250 mm. The air gap between the transmission and receiving coils is 80 mm. The SAS (Solar Array Simulator) software can simulate the output characteristics of the PV panel shown in Fig. 2 and can evaluate the MPPT control tracking performance when comparing the P_{PV} of the SAS with the set P_{MPP}. The parameters used in the simulations and experiments are shown in TABLE I. In (a), the parameters of the PV panel are represented, and the switching frequency of the DC/DC converter is set to f_{dc}, the minute variation of the duty ratio used in the MPTT control is set to Δd, and the sampling time to update the duty ratio is set to duty sample. In (b), the parameters of DWPT are represented, and the switching frequency of the inverter is set to f_0. In (c), the resonant elements of the Double-LCC topology, which is the compensation topology of the WPT used in this paper, are represented.

VI. Verification of PV+DWPT System

A. Comparison of simulation and experiment in PV section

Under the conditions shown in Fig. 9, measurements were made for 10 seconds, and the solar irradiance was changed from 1000 W/m^2 to 500 W/m^2 at exactly 5 second. The simulation results are shown in Fig. 10 and the experimental results in Fig. 11. In both Fig. 10 and Fig. 11, it was confirmed that in (a), P_{PV} can follow P_{MPP} even when solar irradiance changes. However, in Fig. 11, it was confirmed that P_{PV} temporarily exceeded P_{MPP} due to switching noise at intervals of 0.1 second, the sampling time, when the duty ratio was updated. This is because the output characteristics of the PV panel in the experiment shown in (b) of Fig. 9 were graphed by measuring the average values of P_{PV} and I_{PV} for each value of V_{PV}, and the maximum power point of P_{PV} is P_{MPP}.The MPPT efficiency was calculated in (b) of Fig. 10 and 11 using (8), and the MPPT efficiency was almost 100.0 %, except at exactly 5 second when the solar iradiance changed abruptly. The average value of η_{MPPT} at 1000 W/m^2 in the

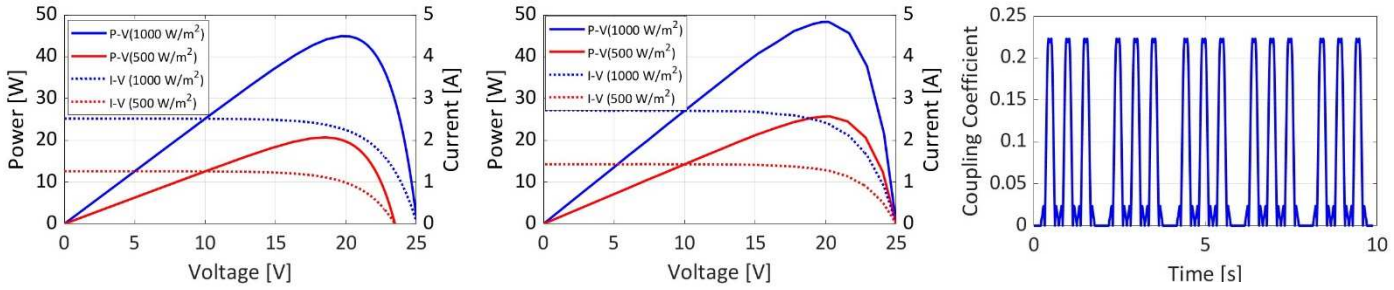

(a) P-V, I-V curve (simulation) (b) P-V, I-V curve (experiment) (c) Coupling Coefficient (0 ~ 10 second)

Fig. 9. PV panel design and solar irradiance settings for the PV+DWPT system, and the coupling coefficient transition between the transmission and receiving coils.

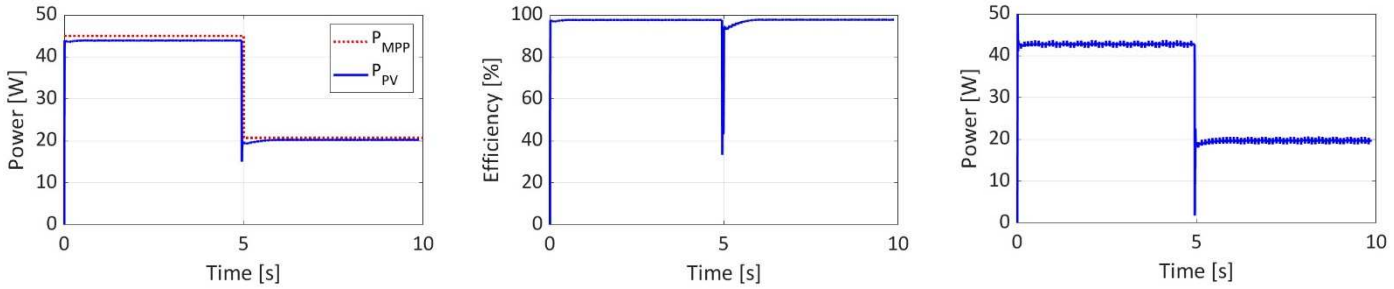

(a) P_{PV} tracking against P_{MPP} (b) MPPT control efficiency of P_{PV} against P_{MPP} (c) PV power after DC/DC converter (P'_{PV})

Fig. 10. Result of power after MPPT control and power conversion by DCDC converter in the proposed PV+DWPT system (simulation)

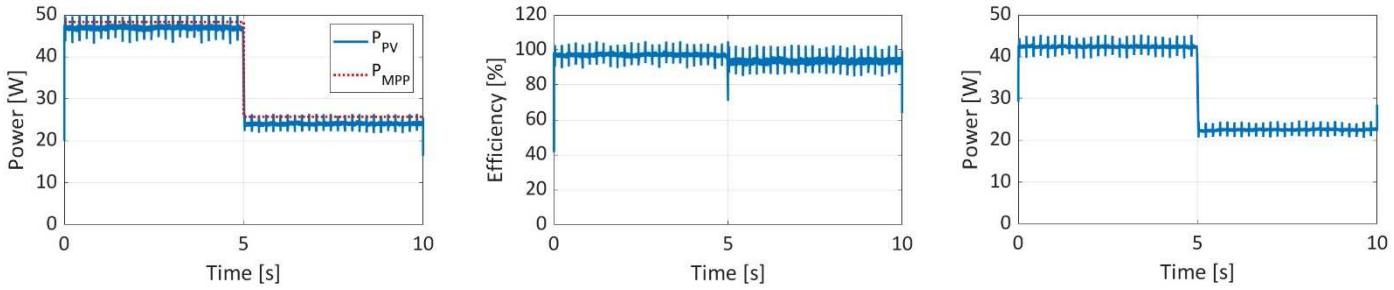

(a) P_{PV} tracking against P_{MPP} (b) MPPT control efficiency of P_{PV} against P_{MPP} (c) PV power after DC/DC converter (P'_{PV})

Fig. 11. Result of power after MPPT control and power conversion by DCDC converter in the proposed PV+DWPT system (experiment)

experiment was 96.1 %, although it temporarily exceeded 100.0 % due to noise.

$$\eta_{MPPT} = \frac{P_{PV}}{P_{MPP}} \tag{8}$$

And (c) in Fig. 10 and 11 shows the amount of power in P'_{PV}. The calculation of power conversion efficiency by the DC/DC converter is shown in (9). The average value of η_{DCDC} under steady state conditions at 1000 W/m^2 of solar irradiance was 91.6 % in the experiment.

$$\eta_{DCDC} = \frac{P'_{PV}}{P_{PV}} \tag{9}$$

B. *Comparison of simulation and experiment in DWPT section*

The simulation results verified under the conditions of Fig. 9 in the DWPT section after the DC bus are shown in Fig. 12, and the experimental results are shown in Fig. 13. The waveform of the coupling coefficient in (c) of Fig. 9 was created based on the coupling coefficient values between Tx2 and Rx. Rx was moved on the static Tx2 by a minute amount in accordance with the position coordinates, and the coupling coefficient for each position coordinate was measured when both were static. Based on this, the coupling coefficients were graphed when Rx was assumed to pass over Tx2, converted from the speed of the receiving coil, 7 km/h. Then, the coupling coefficient when it was assumed that the Rx moved from Tx1 ~ Tx3 was graphed with three consecutive coupling coefficients when it passed through Tx2. Therefore, during the 10 seconds measurement, an Rx with a speed of 7 km/h made two and a half round trips on Tx1 ~ Tx3. However, the simulation and experiment do not perfectly match the overall circuit design, including the coupling coefficient values, time axis, and resonance parameters of Tx1 to Tx3, resulting in a misalignment of the time axis and power when comparing the two. Based on the above, comparing Fig. 12 and Fig. 13, it can be seen that in (a), the input power P_{dc} to the DC bus changes in accordance with the power transmission of the DWPT. In addition, it can be seen that in 0 ~ 5 second, P_{dc} is almost always positive, although there is a primary negative area in Fig. 13, and it is always positive in Fig. 12.This indicates that DWPT can be performed with PV power alone, without requiring power supply from the grid. On the other hand, at 5 ~ 10 second, both Fig. 12 and Fig. 13 show that the power values are temporarily negative. This indicates that $P_{dc} < P_{in}$ and that the grid is supplying the missing power through the DC bus. In (b), P_{in} is the input power of DWPT, and in (c), P_{out} is the output power of DWPT. In Fig. 12, the P_{in} and P_{out} power quantities are repeated equally every 2 seconds. On the other hand, in Fig. 13, not only is the amount of power when passing through Tx1 less than when passing through the other two, but also the amount of power in P_{in} and P_{out} is different from that in Fig. 12. This may be due to design deviations in the simulations and experiments described earlier, or measurement errors. Also, when the coupling coefficient is 0, almost no power is transmitted in Fig. 12, whereas in Fig. 13, power is supplied to the circuit, although at a small power level. This is due to the presence of line resistance and internal resistance of the resonance element in the experimental circuit, but the characteristic that power transmission stops when the coupling coefficient of the Double-LCC topology is 0 was confirmed in Fig. 12 and 13.

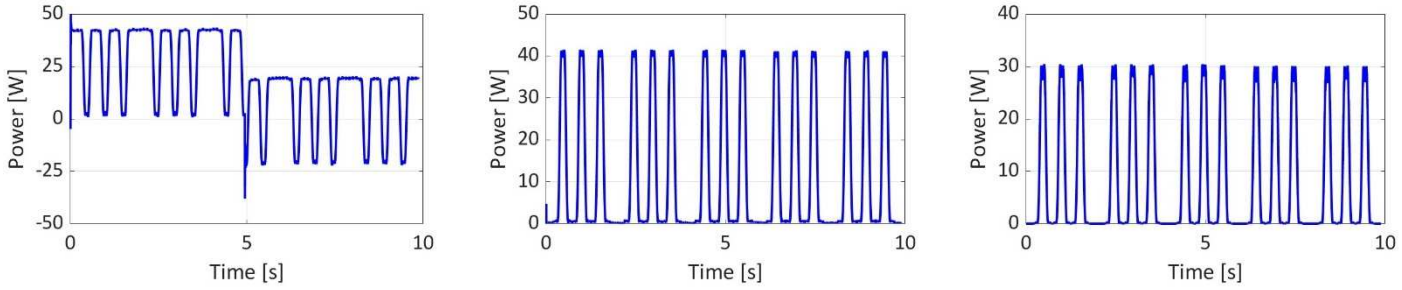

(a) DC bus input power (P_{dc}) (b) Input power of DWPT (P_{in}) (c) Output power of DWPT (P_{out})

Fig. 12. Input power at DC bus and input and output power at DWPT in a PV+DWPT system (simulation)

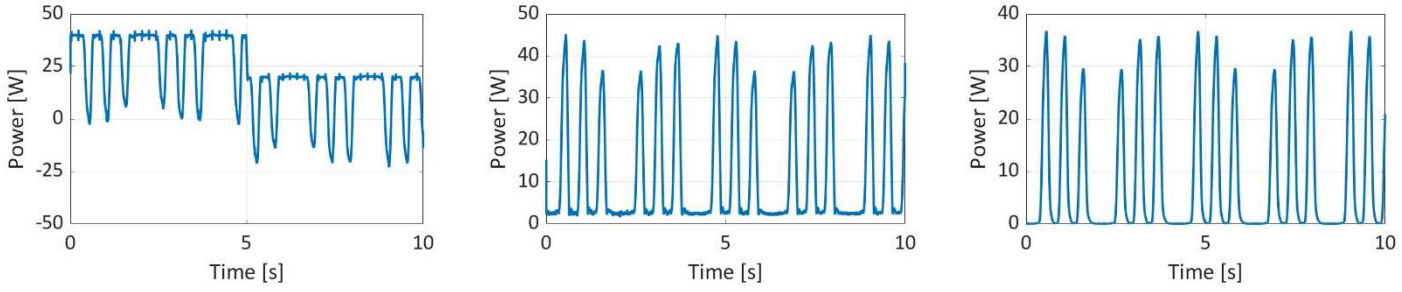

(a) DC bus input power (P_{dc}) (b) Input power of DWPT (P_{in}) (c) Output power of DWPT (P_{out})

Fig. 13. Input power at DC bus and input and output power at DWPT in a PV+DWPT system (experiment)

C. *Amount of power and conversion efficiency of each part of the proposed PV+DWPT experimental system at static*

TABLE II shows the amount of power in each part of the experimental system when the solar irradiance is 1000 W/m^2 and the receiving coil Rx is static in the center of the transmission coil Tx2, and the power conversion efficiency in each part of the system is shown in TABLE III. The calculation method for each conversion efficiency is shown in (10) and (11).

$$\eta_{SWPT} = \frac{P_{out}}{P_{in}} \tag{10}$$

$$\eta_{PV+DWPT} = \eta_{MPPT} \times \eta_{DCDC} \times \eta_{SWPT} \tag{11}$$

From TABLE III, the MPPT conversion efficiency, the DC/DC converter conversion efficiency, and the power conversion efficiency between the transmission and receiving coils in the SWPT section were shown. The power conversion efficiency until the power generated by the PV is finally fed to the battery of the BEV is $\eta_{PV+DWPT}$, indicating that the power conversion efficiency of the entire proposed system is 76.4 %.

TABLE Ⅱ. AMOUNT OF ELECTRICITY FOR EACH PART IN A PV+DWPT SYSTEM

P_{MPP} [W]	P_{PV} [W]	P'_{PV} [W]	P_{dc} [W]	P_{in} [W]	P_{out} [W]
48.3	46.4	42.5	- 3.0	45.5	39.5

TABLE Ⅲ. POWER CONVERSION EFFICIENCY OF VARIOUS PARTS IN A PV+DWPT SYSTEM

η_{MPPT} [%]	η_{DCDC} [%]	η_{SWPT} [%]	$\eta_{PV+DWPT}$ [%]
96.1	91.6	86.8	76.4

VII. CONCLUSION

In this paper, a basic study of a PV+DWPT (grid-connected) circuit configuration was conducted and verified through simulation and experiment. Simulation and experimental results show that the DWPT was able to use MPPT control when generating power with PV, while keeping it tracked near the MPP of PV power. In addition, in a PV+DWPT system, DWPT can be performed using only PV power when PV power generation is sufficient, and power can be supplied from the grid only when PV power generation is insufficient. In this way, when the amount of electricity generated by the PV is insufficient to perform DWPT, DWPT can be performed with a stable amount of electricity by supplementing the deficient amount of electricity from the grid. Therefore, the PV+DWPT system can reduce the consumption of grid power compared to DWPT without PV. The experimental results show that the proposed system as a whole has a power conversion efficiency of 76.4 %, which indicates that BEVs can effectively run while using DWPT with power derived from renewable energy sources. In conclusion, the usefulness and feasibility of the proposed PV+DWPT system were demonstrated. In addition, in the system under consideration, there is a need for the grid to adjust all the voltage fluctuations in the DC bus caused by PV, which is unstable power, and DWPT, which is a variable load. Therefore, the grid, which plays the role of regulating the power, is expected to bear a heavy burden. However, since most of the power generated by the PV can be consumed on nearby roads, transmission losses are expected to be small and the amount of power supplied by the grid can be significantly reduced. Therefore, the overall burden on the grid is considered to be low, and the PV+DWPT system studied in this paper is considered to be useful. Based on the above, future considerations for this proposed system design include improving the power conversion efficiency $\eta_{PV+DWPT}$ of the entire proposed system. In addition, for the PV+DWPT (grid-connected) system, the optimal PV installation capacity at the location where the PV+DWPT system is installed and measures to reduce the burden on the grid are also considered.

REFERENCES

[1] A. C. Bagchi, A. Kamineni, R. A. Zane and R. Carlson, "Review and Comparative Analysis of Topologies and Control Methods in Dynamic Wireless Charging of Electric Vehicles," in IEEE Journal of Emerging and Selected Topics in Power Electronics, vol. 9, no. 4, pp. 4947-4962, Aug. 2021.

[2] Z. Zhou, L. Zhang, Z. Liu, Q. Chen, R. Long and H. Su, "Model Predictive Control for the Receiving-Side DC–DC Converter of Dynamic Wireless Power Transfer," in IEEE Transactions on Power Electronics, vol. 35, no. 9, pp. 8985-8997, Sept. 2020.

[3] R. Tavakoli, T. Shabanian, E. M. Dede, C. Chou and Z. Pantic, "EV Misalignment Estimation in DWPT Systems Utilizing the Roadside Charging Pads," in IEEE Transactions on Transportation Electrification, vol. 8, no. 1, pp. 752-766, March 2022.

[4] A. N. Azad, A. Echols, V. A. Kulyukin, R. Zane and Z. Pantic, "Analysis, Optimization, and Demonstration of a Vehicular Detection System Intended for Dynamic Wireless Charging Applications," in IEEE Transactions on Transportation Electrification, vol. 5, no. 1, pp. 147-161, March 2019.

[5] R. Tavakoli and Z. Pantic, "Analysis, Design, and Demonstration of a 25-kW Dynamic Wireless Charging System for Roadway Electric Vehicles," in IEEE Journal of Emerging and Selected Topics in Power Electronics, vol. 6, no. 3, pp. 1378-1393, Sept. 2018.

[6] A. Mahesh, B. Chokkalingam and L. Mihet-Popa, "Inductive Wireless Power Transfer Charging for Electric Vehicles–A Review," in IEEE Access, vol. 9, pp. 137667-137713, 2021.

[7] S. Zou, O. C. Onar, V. Galigekere, J. Pries, G. -J. Su and A. Khaligh, "Secondary Active Rectifier Control Scheme for a Wireless Power Transfer System with Double-Sided LCC Compensation Topology," IECON 2018 - 44th Annual Conference of the IEEE Industrial Electronics Society, 2018, pp. 2145-2150.

[8] T. Theodoropoulos et al., "Impact of dynamic EV wireless charging on the grid," 2014 IEEE International Electric Vehicle Conference (IEVC), 2014, pp. 1-7.

[9] R. Zeng, V. Galigekere, O. Onar and B. Ozpineci, "Optimized Renewable Energy Integration for EV High-Power Dynamic Wireless Charging Systems," 2021 IEEE Power & Energy Society Innovative Smart Grid Technologies Conference (ISGT), 2021, pp. 1-5.

[10] K. Kumar, K. V. V. S. R. Chowdary, P. Sanjeevikumar and R. Prasad, "Analysis of Solar PV Fed Dynamic Wireless Charging System for Electric Vehicles," IECON 2021 – 47th Annual Conference of the IEEE Industrial Electronics Society, 2021, pp. 1-6.

[11] P. S. R. Nayak, K. Kamalapathi, N. Laxman and V. K. Tyagi, "Design and Simulation Of BUCK-BOOST Type Dual Input DC-DC Converter for Battery Charging Application in Electric Vehicle," 2021 International Conference on Sustainable Energy and Future Electric Transportation (SEFET), 2021, pp. 1-6.

[12] A. Babaki, S. Vaez-Zadeh, M. F. Moghaddam and A. Zakerian, "A Novel Multi-Objective Topology for In-Motion WPT Systems with an Input DG Source," 2019 10th International Power Electronics, Drive Systems and Technologies Conference (PEDSTC), 2019, pp. 787-792.